GRAS SAF Report 07
Ref: SAF/GRAS/METO/REP/GSR/007
Web: www.grassaf.org
Date: 1 October 2008

The EUMETSAT Network of Satellite Application Facilities

GRAS SAF
GRAS Meteorology

GRAS SAF Report 07

# Abel integral calculations in ROPP

Huw Lewis

*Met Office, UK*

## Document Author Table

| | *Name* | *Function* | *Date* | *Comments* |
|---|---|---|---|---|
| ***Prepared by:*** | H. Lewis | GRAS SAF Project Team | 1 October 2008 | |
| ***Reviewed by:*** | S. Syndergaard | GRAS SAF Project Team | 7 October 2008 | |
| ***Approved by:*** | K.B. Lauritsen | GRAS SAF Project Manager | 17 October 2008 | |

## Document Change Record

| *Issue/Revision* | *Date* | *By* | *Description* |
|---|---|---|---|
| Version 1.0 | 1 Oct 2008 | HL | First version |

## GRAS SAF Project

The GRAS SAF is a EUMETSAT-funded project responsible for operational processing of GRAS radio occultation data from the Metop satellites. The GRAS SAF delivers bending angle, refractivity, temperature, pressure, and humidity profiles in near-real time and offline for NWP and climate users. The offline profiles are further processed into climate products consisting of gridded monthly zonal means of bending angle, refractivity, temperature, humidity, and geopotential heights together with error descriptions.

The GRAS SAF also maintains the Radio Occultation Processing Package (ROPP) which contains software modules that will aid users wishing to process, quality-control and assimilate radio occultation data from any radio occultation mission into NWP and other models.

The GRAS SAF Leading Entity is the Danish Meteorological Institute (DMI), with Cooperating Entities: i) European Centre for Medium-Range Weather Forecasts (ECMWF) in Reading, United Kingdom, ii) Institut D'Estudis Espacials de Catalunya (IEEC) in Barcelona, Spain, and iii) Met Office in Exeter, United Kingdom. To get access to our products or to read more about the project please go to http://www.grassaf.org.

## Abstract

The ROPP pre-processor module `ropp_pp` includes routines to perform an Abel transform to derive a bending angle profile from model refractivity data and invert a corrected bending angle profile to derive refractivity. This report describes the inverse Abel and forward Abel transform calculations included within ROPP. The sensitivity of `ropp_pp` and `ropp_fm` results to the choice of algorithm used is discussed.

# 1 Background

The bending angle can be derived from the refractive index $n$ by the Abel integral (Fjeldbo et al., 1971; Melbourne et al., 1994; Kursinski et al., 1997).

$$\begin{aligned}\alpha(a) = -2\int_{r_t}^{\infty} d\alpha &= -2a\int_{r_t}^{\infty} \frac{1}{\sqrt{r^2n^2 - a^2}} \frac{d\ln(n)}{dr} dr \\ &= -2a\int_{a}^{\infty} \frac{1}{\sqrt{x^2 - a^2}} \frac{d\ln(n)}{dx} dx \ .\end{aligned} \tag{1.1}$$

The second expression is obtained by substituting $x = nr$. The negative sign in Equation 1.1 follows the convention that bending towards the Earth's surface is positive.

Equation 1.1 can be inverted by the Abel transform, so that for a given corrected bending angle profile $\alpha(a)$ the refractive index is expressed as,

$$n(r) = \exp\left[\frac{1}{\pi}\int_{x}^{\infty} \frac{\alpha(a)}{\sqrt{a^2 - x^2}} da\right] \tag{1.2}$$

To reduce the influence of the infinite upper boundary condition on the inversion of a finite depth bending angle profile, the corrected bending angle profile is extended above the highest measurement impact parameter using a climatological profile (e.g. Hedin, 1991).

Both Equations 1.1 and 1.2 may be generalised as

$$f(z) = A\int_{z}^{\infty} \frac{g(y)}{\sqrt{y^2 - z^2}} dy \tag{1.3}$$

where a profile $f(z)$ can be derived from a profile $g(y)$ where $z$ and $y$ are known height scales and $A$ is a constant. For the forward Abel (Equation 1.1), $f(z) \rightarrow \alpha(a)$, $g(y) \rightarrow d\ln(n)/dr$, $A \rightarrow -2a$. For the inverse Abel (Equation 1.2), $f(z) \rightarrow \ln n(r)$, $g(y) \rightarrow \alpha(a)$, $A \rightarrow 1/\pi$

The `ropp_pp` module includes algorithms to solve the forward Abel (Equation 1.1) and inverse Abel (Equation 1.2). Two different algorithms to solve the Abel integral have been tested as part of the development of the `ropp_pp` module. In both cases the algorithms solve the generalised Abel integral (Equation 1.3) by assuming that variable $g(y)$ can be approximated as a known function of $y$ between successive observation levels, for which an analytical solution to the Abel integral can be found. Equations 1.1 and 1.2 are then solved by summing contributions from the solutions to the known sub-integrals for each observation level.

A forward Abel transform operator developed by the GRAS SAF is currently used as part of the forward model module `ropp_fm` included in ROPP (`ropp_fm_abel`) for the calculation of bending angle profiles from refractivity derived from background data. This routine has now been implemented in the `ropp_pp` module together with its inverse. It is assumed that profiles vary exponentially as a function of height between data levels, so that the Abel

integral is approximated in terms of the error function. This approach is referred to as the 'exponential' algorithm in this report.

An alternative algorithm was developed by Michael Gorbunov (whilst a visiting scientist with the GRAS SAF). It is assumed that profiles vary linearly between data levels, so that the Abel integral can be solved analytically. This approach is referred to as the 'linear' algorithm in this report.

## 1.1 'Exponential' algorithms

### 1.1.1 Forward Abel `ropp_pp_abel_exp`

Equation 1.1 is simplified by approximating

$$\frac{d\ln(n)}{dx} \approx 10^{-6}\frac{dN}{dx}$$

which is valid because the refractivity is small, and

$$\sqrt{x^2-a^2} \approx \sqrt{2a(x-a)}$$

This is valid because the refractivity scale height is small compared to the radius of the Earth. This gives

$$\alpha(a) = -\sqrt{2a}10^{-6}\int_a^\infty \frac{dN/dx}{\sqrt{x-a}}dx \tag{1.4}$$

Assuming that refractivity varies exponentially with $x = nr$ between observation levels leads to an estimate for the refractivity gradient between the $j$ and $j+1$ levels,

$$N = N_j \exp(-k_j(x-x_j)) \tag{1.5}$$

$$\frac{dN}{dx} = -k_j N_j \exp(-k_j(x-x_j)) \tag{1.6}$$

with

$$k_j = \frac{\ln(N_j/N_{j+1})}{(x_{j+1}-x_j)} \tag{1.7}$$

The value of $k_j$ is required to be positive, so a minimum positive value of $k_j^{min} = 10^{-6}$ is assumed.

Substituting Equation 1.6 into 1.13 leads to an expression for the bending between the $j$ and $j+1$ levels,

$$\Delta\alpha_j = 10^{-6}k_j N_j \exp(k_j(x_j-a))\sqrt{2a}\int_{x_j}^{x_{j+1}} \frac{\exp(-k_j(x-a))}{(x-a)^{1/2}}dx \tag{1.8}$$

The lowest usable level to compute bending angle is defined as that level where the impact parameter first decreases with decreasing height towards the surface. This will occur in conditions of super-refraction.

By change of variables, $t = (k_j(x-a))^{1/2}$,

$$\Delta\alpha_j = 10^{-6}\sqrt{2\pi a k_j}N_j \exp(k_j(x_j-a))\left[\text{erf}\left(\sqrt{k_j(x_{j+1}-a)}\right) - \text{erf}\left(\sqrt{k_j(x_j-a)}\right)\right] \quad (1.9)$$

where the error function `erf` is defined as

$$erf(x) = \frac{2}{\sqrt{\pi}}\int_0^x e^{-t^2}dt \quad (1.10)$$

The error function terms are computed in `ropp_pp_abel_exp` using a polynomial approximation (Abramowitz and Stegun, 1965). Ray bending above the model top is accounted for by extrapolating when $j+1$ is the top of the profile and evaluating

$$\Delta\alpha_{top} = 10^{-6}\sqrt{2\pi a k_j}N_j \exp(k_j(x_j-a))\left[1 - \text{erf}\left(\sqrt{k_j(x_j-a)}\right)\right] \quad (1.11)$$

The total bending angle $\alpha_i$ at a certain impact parameter $a_i$ is then found by summing contributions calculated using Equation 1.9 between $a_i$ and the top of the background profile.

$$\alpha_i = -2a_i\sum_{j=i}^{n}\Delta\alpha_j \quad (1.12)$$

### 1.1.2 Inverse Abel `ropp_pp_invert_exp`

Equation 1.2 can be solved in a similar manner. Assuming that bending angle varies exponentially with $a$ between observation levels gives,

$$\alpha = \alpha_j \exp(-k_{\alpha_j}(a-a_j)) \quad (1.13)$$

with

$$k_{\alpha_j} = \frac{\ln \alpha_j/\alpha_{j+1}}{(a_{j+1}-a_j)} \quad (1.14)$$

By substituting Equation 1.13 into Equation 1.2 leads to an expression for the change in refractive index between the $j$ and $j+1$ levels,

$$\Delta(\ln n)_j = \frac{1}{\sqrt{2x\pi}}\alpha_j \exp(k_{\alpha_j}(a_j-x))\int_{a_j}^{a_{j+1}}\frac{\exp(-k_{\alpha_j}(a-x))}{(a-x)^{1/2}}da \quad (1.15)$$

Finally by change of variables, $t = (k_{\alpha_j}(a-x))^{1/2}$,

$$\Delta(\ln n)_j = \frac{1}{\sqrt{2\pi x k_{\alpha_j}}}\alpha_j \exp(k_{\alpha_j}(a_j-x))\left[\text{erf}\left(\sqrt{k_{\alpha_j}(a_{j+1}-x)}\right) - \text{erf}\left(\sqrt{k_{\alpha_j}(a_j-x)}\right)\right] \quad (1.16)$$

The refractive index $n_i$ at a certain impact parameter $a_i$ is then found by summing contri-

butions calculated using Equation 1.16 between $a_i$ and the top of the background profile.

$$n_i = \exp\left[\frac{1}{\pi}\sum_{j=i}^{n}\Delta(\ln n)_j\right] \tag{1.17}$$

## 1.2 'Linear' algorithms

Assuming that $\alpha(a)$ varies linearly between observation levels,

$$\alpha(x) = \frac{x-a_j}{a_{j+1}-a_j}\alpha_{j+1} + \frac{a_{j+1}-x}{a_{j+1}-a_j}\alpha_j \tag{1.18}$$

leads to an expression for the Abel transform

$$\ln n(r) = \sum_{j=1}^{n}\int_{a_j}^{a_{j+1}} A(x,a)\left[\frac{x-a_j}{a_{j+1}-a_j}\alpha_{j+1} + \frac{a_{j+1}-x}{a_{j+1}-a_j}\alpha_j\right]dx \tag{1.19}$$

with

$$A(x,a) = -\frac{1}{\pi(x^2-a^2)^{1/2}} \tag{1.20}$$

The integral in Equation 1.19 can be solved analytically. Defining $\Delta a_j = a_{j+1} - a_j$,

$$\frac{\alpha_{j+1}}{\Delta a_j}\int_{a_j}^{a_{j+1}} A(x,a)(x-a_j)dx = -\frac{\alpha_{j+1}}{\pi\Delta a_j}\left[\sqrt{a_{j+1}^2-a^2} - \sqrt{{a_j}^2-a^2} - a_j\ln\left(\frac{a_{j+1}+\sqrt{a_{j+1}^2-a^2}}{a_j+\sqrt{a_j^2-a^2}}\right)\right] \tag{1.21}$$

$$\frac{\alpha_j}{\Delta a_j}\int_{a_j}^{a_{j+1}} A(x,a)(a_{j+1}-x)dx = -\frac{\alpha_j}{\pi\Delta a_j}\left[\sqrt{a_{j+1}^2-a^2} - \sqrt{{a_j}^2-a^2} - a_{j+1}\ln\left(\frac{a_{j+1}+\sqrt{a_{j+1}^2-a^2}}{a_j+\sqrt{a_j^2-a^2}}\right)\right] \tag{1.22}$$

These expressions can be combined to give the change in refractive index between the j and j+1 levels. The refractive index at an impact parameter $a_i$ is then given by the sum of contributions due to the change in refractive index from $j = i$ to the top of the atmosphere.

$$n_i = \exp\left[\frac{1}{\pi}\sum_{j=i}^{n}\Delta(\ln n)_j\right] \tag{1.23}$$

where

$$\Delta(\ln n)_j = \frac{1}{\pi\Delta a_j}\left[\left(\alpha_j a_{j+1} - \alpha_{j+1}a_j\right)\ln\left(\frac{a_{j+1}+\sqrt{a_{j+1}^2-a^2}}{a_j+\sqrt{a_j^2-a^2}}\right) + \left(\alpha_{j+1}-\alpha_j\right)\left(\sqrt{a_{j+1}^2-a^2} - \sqrt{{a_j}^2-a^2}\right)\right] \tag{1.24}$$

The infinite upper boundary condition may be accounted for by adding a further correction term to the summation of refractive index contributions.

$$\Delta(\ln n)_{top} = \frac{\alpha_{top}}{\sqrt{\pi h'}} \exp\left(\frac{a_{top}-a_i}{h}\right)\left[1-\text{erf}\left(\sqrt{\frac{a_{top}-a_i}{h}}\right)\right] \tag{1.25}$$

where $h' = (a_{top}+a_i)/h$ and $h$ is a scale height, computed as $h = -\Delta a/\Delta(\ln\alpha)$ with differences in impact parameter and $\ln\alpha$ estimated across the upper part of the input bending angle profile.

The equivalent analysis can be applied to the Abel transform, assuming that $d\ln(n)/dx$ varies linearly between observation levels. To derive the corresponding solution to Equation 1.1 for the bending angle $\alpha_i$ at impact parameter $a_i$ can be written as a sum of contributions due to change in bending angle $\Delta\alpha_j$ from $j = i$ to the top of the atmosphere. The bending angle contributions at each level $j$ can be expressed in terms of observation impact parameters and the observed gradient of refractive index $d\ln(n)/dx$ at levels $j+1$ and $j$.

$$\alpha_i = -2a_i \sum_{j=i}^{n} \Delta\alpha_j \tag{1.26}$$

where

$$\Delta(\alpha)_j = \tag{1.27}$$
$$\frac{1}{\Delta a_j}\left[\left(dln_j a_{j+1} - dln_{j+1} a_j\right)\ln\left(\frac{a_{j+1}+\sqrt{a_{j+1}^2-a^2}}{a_j+\sqrt{a_j^2-a^2}}\right) + \left(dln_{j+1}-dln_j\right)\left(\sqrt{a_{j+1}^2-a^2}-\sqrt{{a_j}^2-a^2}\right)\right]$$

The correction term for the infinite upper boundary condition is

$$\Delta(\alpha)_{top} = \frac{dln_{top}\sqrt{\pi}}{\sqrt{h'}} \exp\left(\frac{a_{top}-a_i}{h}\right)\left[1-\text{erf}\left(\sqrt{\frac{a_{top}-a_i}{h}}\right)\right] \tag{1.28}$$

where $h' = (a_{top}+a_i)/h$ and $h$ is a scale height, computed as $h = -(\Delta a)N/\Delta N$.

Note that in contrast to the exponential assumption algorithms, the linear algorithms are designed to compute output (bending angle or refractivity) profiles on the same impact parameter levels as the input (refractivity or bending angle) profile. The exponential algorithm enables profiles to be computed on a different set of output impact parameters if required. This is utilised in the ROPP forward model for example, where bending angle profiles on observation impact parameter levels are directly computed from refractivity values defined on model background levels. At present, the result of the linear algorithm must be interpolated onto a different set of impact parameter levels if required. Further development work may be required to enable the linear algorithm to be used in a more flexible way.

# 2 Abel integral results

## 2.1 Difference between 'linear' and 'exponential' algorithms

Figure 2.1 shows the sensitivity of bending angle profiles computed from sample refractivity profiles to calculation using the 'exponential' and 'linear' forward Abel transform algorithms. Note that no quality checks were performed in selecting the sample profiles, so some unphysical profiles are also processed. In most cases relative differences of less than 0.1% in bending angle up to 40 km occurs between the different algorithms. This results from errors in the assumption of linear and exponential change of refractivity with between observation levels used to compute the bending angle profiles. Some input refractivity profiles in Figure 2.1 demonstrate more complicated structures and the relative differences between the results of the two algorithms are much larger. Towards the top of each profile, relative errors increase up to a maximum of about 15% ($\approx 10^7$ rad). This results from different methods to account for ray bending above the top of the observed profile.

Equivalent profiles in Figure 2.2 illustrate the sensitivity of refractivity profiles computed from the same sample bending angl profiles to calculation using the 'exponential' and 'linear' inverse Abel algorithms. The relative errors in refractivity resulting from the different algorithms are typically a factor of 10 smaller than for bending angle.

## 2.2 Consistency of forward Abel and inverse Abel routines

Figures 2.3 and 2.4 illustrate the errors in incurred in processing refractivity and bending angle data using the forward Abel and inverse Abel routines. In Figure 2.3 a series of computed bending angle profiles are compared with input observed data. The computed profiles result from running the inverse Abel on the input bending angles to obtain a refractivity profile and then performing the forward Abel transform back to bending angle. Results using the 'linear' and the 'exponential' algorithms are plotted. Similarly, Figure 2.4 compares observed refractivity data with the result of applying the forward Abel and inverse Abel on those profiles. In both case, errors are generally very small ($\approx 0.1\%$) for standard profiles up to about 30 km. Differences increase with height further aloft. The 'exponential' algorithms lead to larger differences at lower altitudes than the 'linear' algorithms.

## 2.3 Sensitivity of ionospheric correction results

The inverse Abel and forward Abel transform are used in `ropp_pp` as part of the ionospheric correction of L1 and L2 channel bending angles to corrected bending angle and subsequent calculation of refractivity. The ionospheric correction method is described by Gorbunov (2002). The method aims to combine measured and climataological bending an-

gle data and reduce noise by the application of statistical optimization. The forward Abel transform is used to retrieve a model bending angle profile from MSIS refractivity data. The inverse Abel is used to compute a refractivity profile from the corrected bending angles.

Figure 2.5 demonstrates the level of agreement between the ionospheric correction processing conducted using `ropp_pp` routines with the near-real time (NRT) refractivity products derived by the GRAS SAF using pre-existing software. The corrected refractivity profiles agree to within rounding errors when using the ROPP implementation of the 'linear' Abel integral algorithms. Figure 2.6 shows the difference between the NRT products and ROPP processed refractivity data computed using the 'expoential' Abel integral algorithms. This summarises the sensitivity of profiles to the method of computing the Abel integral. Differences in corrected refractivity increase with height up to a maximum of about 0.5%. Figure 2.7 shows that most of the difference between processing with the 'exponential' and 'linear' algorithms results from the inverse Abel of corrected bending angles. There is a small sensitivity in the ionospheric corrected bending angle profile resulting from the combination of L1 and L2 bending angles with model bending angle data (retrieved from model refractivity using a forward Abel transform) above about 50 km. The relatively small differences in corrected refractivity compared with the results shown in Figures 2.1 and 2.2 can be attributed to the `ropp_pp` processing being applied on a standard grid, with model data contributing above the observed profile top height. This extends the depth of the bending angle profile used in the inverse Abel to retrieve refractivity for example, reducing the impact of sensitivity towards the profile top on results in the height range of interest.

## 2.4 Sensitivity of forward model results

Both the 'exponential' and 'linear' Abel transform algorithms have been applied to retrieve bending angle profiles from background pressure, humidity and temperature data in the `ropp_fm` module. The ROPP forward model first computes a refractivity profile from the background data before an Abel transform is applied to give bending angle. Figures 2.8 and 2.9 show the difference between observed and calculated bending angle profiles using each algorithm. Small scale differences in the O-B bias at low levels in Figure 2.8 can be attributed to the interpolation of bending angles computed using the 'linear' algorithm. At altitudes in excess of about 10 km, the 'linear' algorithm results have a larger negative bias against the observations than achieved using the 'exponential' algorithm. This is because the vertical resolution of the model data used to compute the refractivity profile in the forward model increases with height, from a few metres towards the surface up to several kilometres at the model top. At an altitude of 10 km for example, the resolution of the Met Office model data used in Figure 2.8 is about 1 km and the ECMWF model data used in Figure 2.9 is about 400 m. The assumption that $\ln(n)$ varies linearly between model levels above this altitude becomes less representative, while the exponential assumption is more appropriate. The broader vertical model level resolution for the Met Office model than ECMWF explains why the results of the exponential and linear algorithms differ more for the comparison in Figure 2.8 than in Figure **??**. The standard deviation of differences about the mean is very similar for both algorithms.

These results suggest that the 'exponential' algorithm provided in the `ropp_fm` module is more appropriate for NWP applications. This is because the assumption that refractivity

varies linearly with height is less appropriate as the height interval between impact parameter levels increases. As such, the 'linear' algorithm is suitable for processing RO observations (in `ropp_pp`) for which the height difference between successive impact parameters is about 100 m throughout the profile. The linear approximation is less approprate for processing background model data (in `ropp_fm`) for which the height difference between successive model levels varies between a few metres towards the surface to several kilometres at the model top.

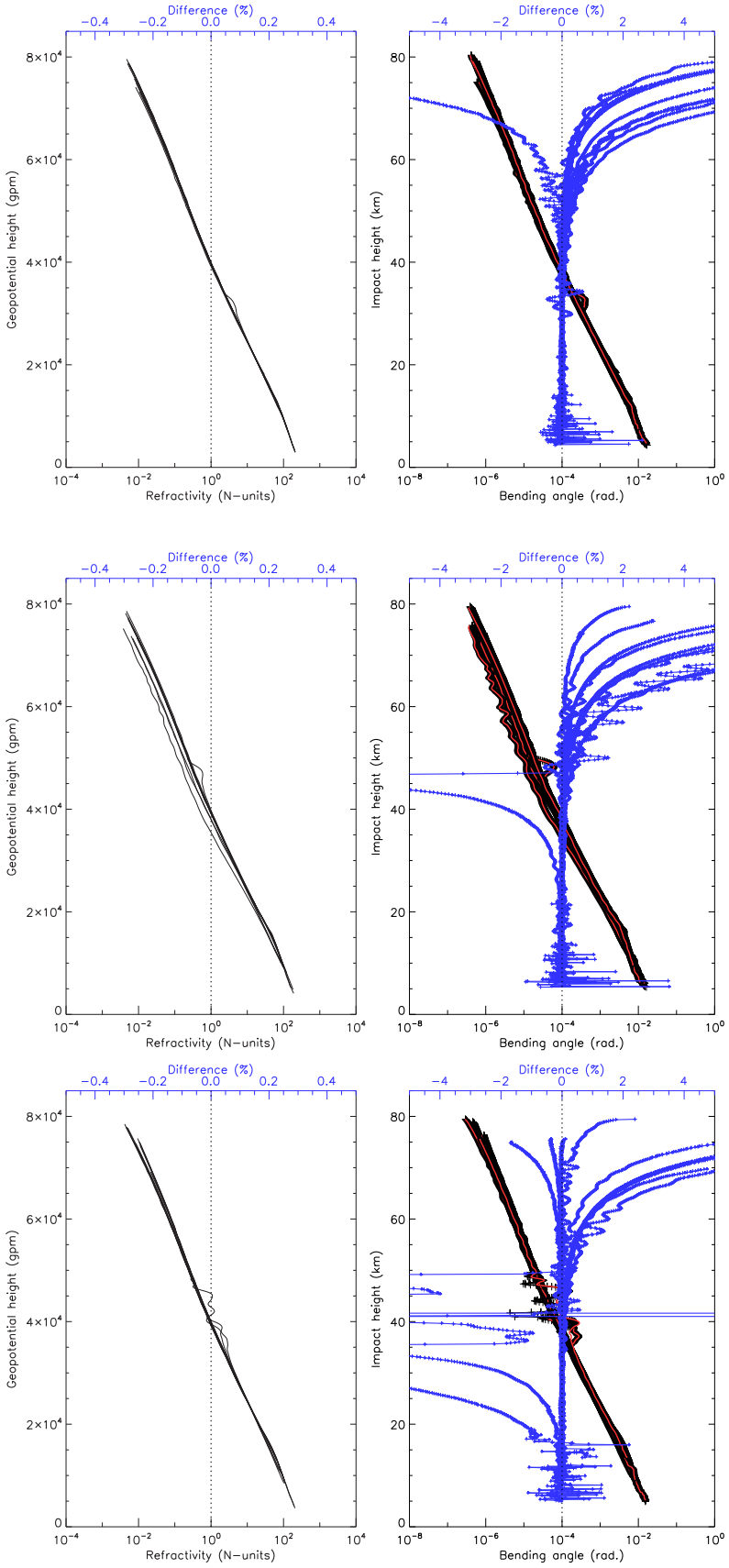


**Figure 2.1:** Sample differences between bending angle profiles computed using ’linear’ (black) ’exponential’ (red) forward Abel transform algorithms.

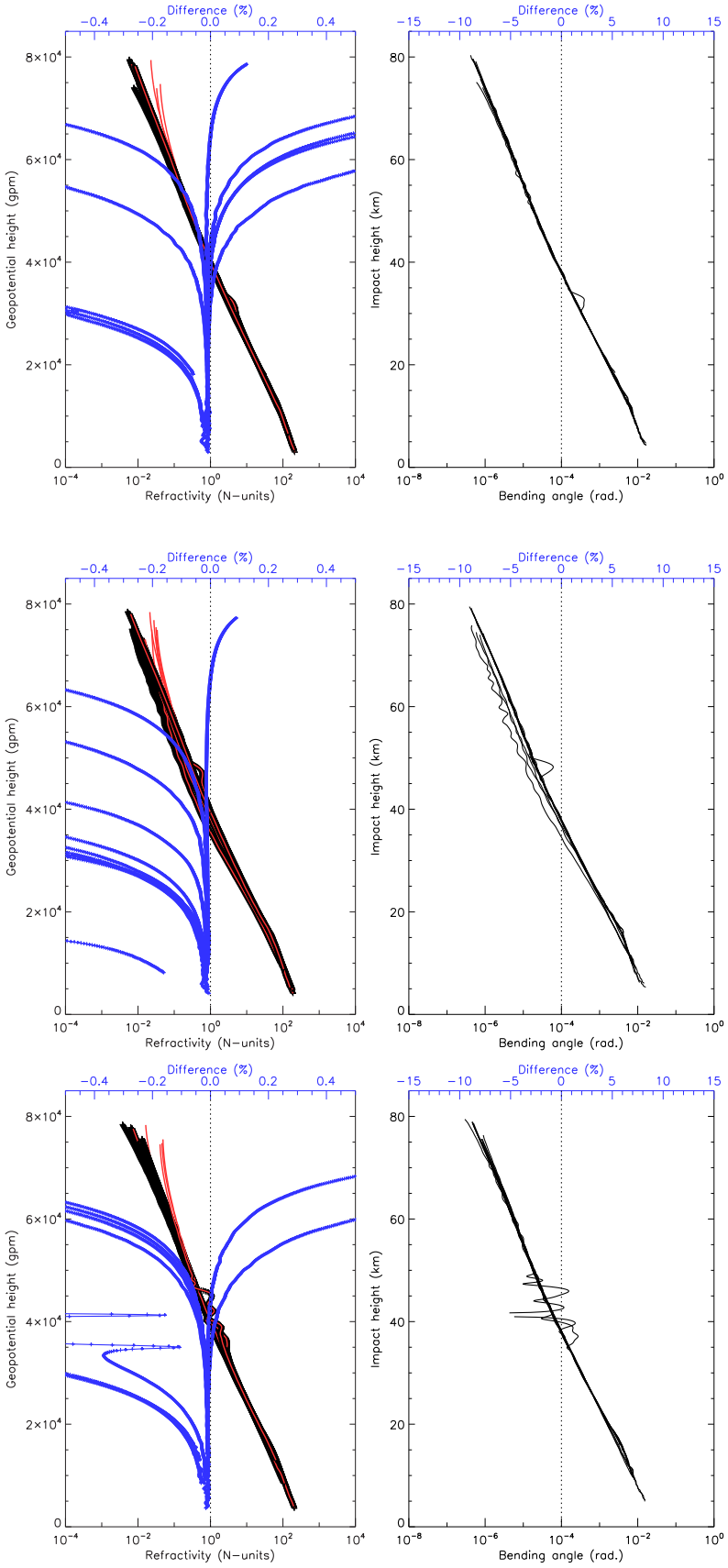


**Figure 2.2:** Sample differences between refractivity profiles computed using 'linear' (black) 'exponential' (red) inverse Abel algorithms.

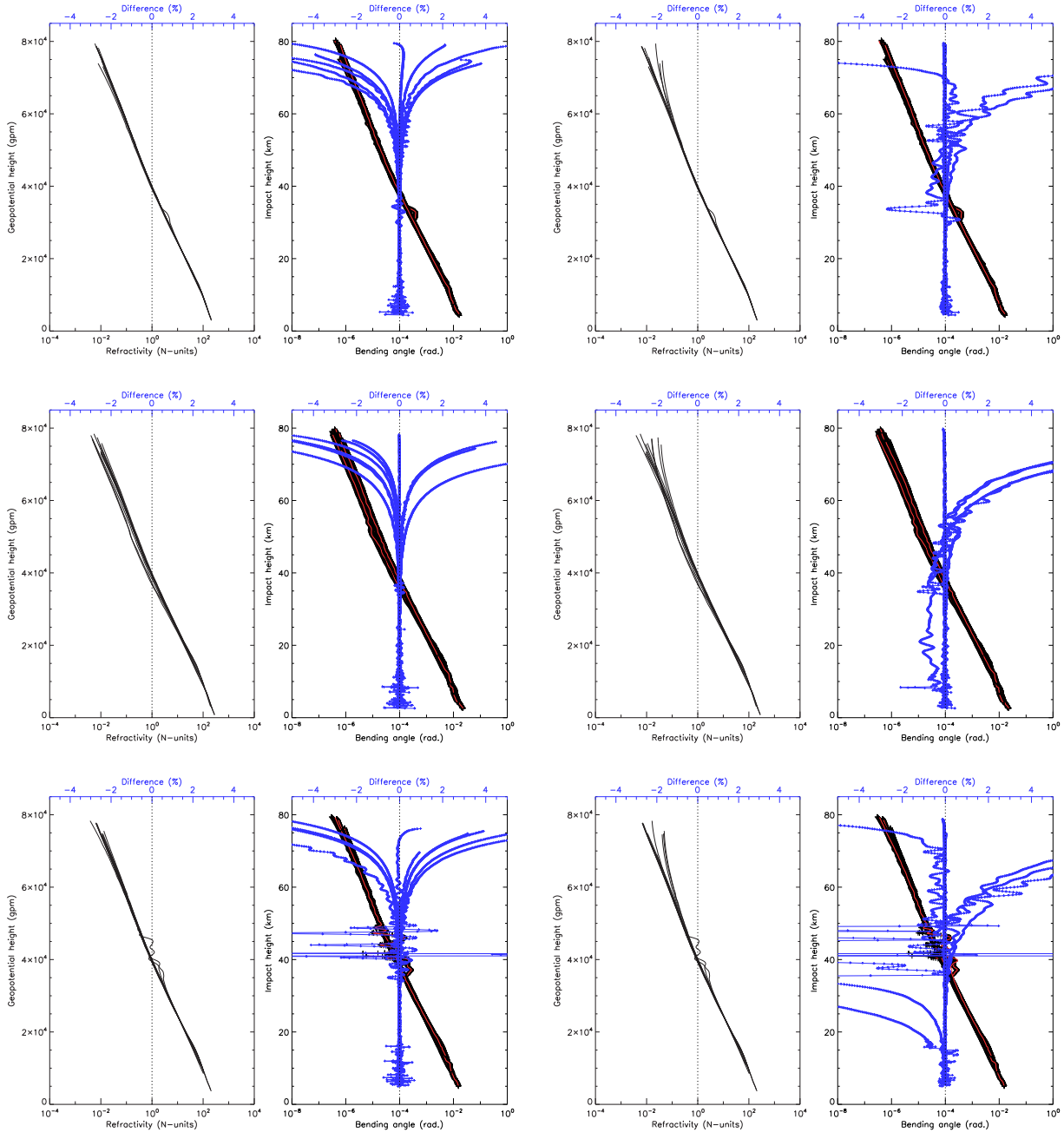


**Figure 2.3:** Sample differences between observed bending angle profiles and the results of successive Abel inversion to refractivity and forward Abel transform back to bending angle. (a) 'linear' algorithms, (b)'exponential' algorithms.

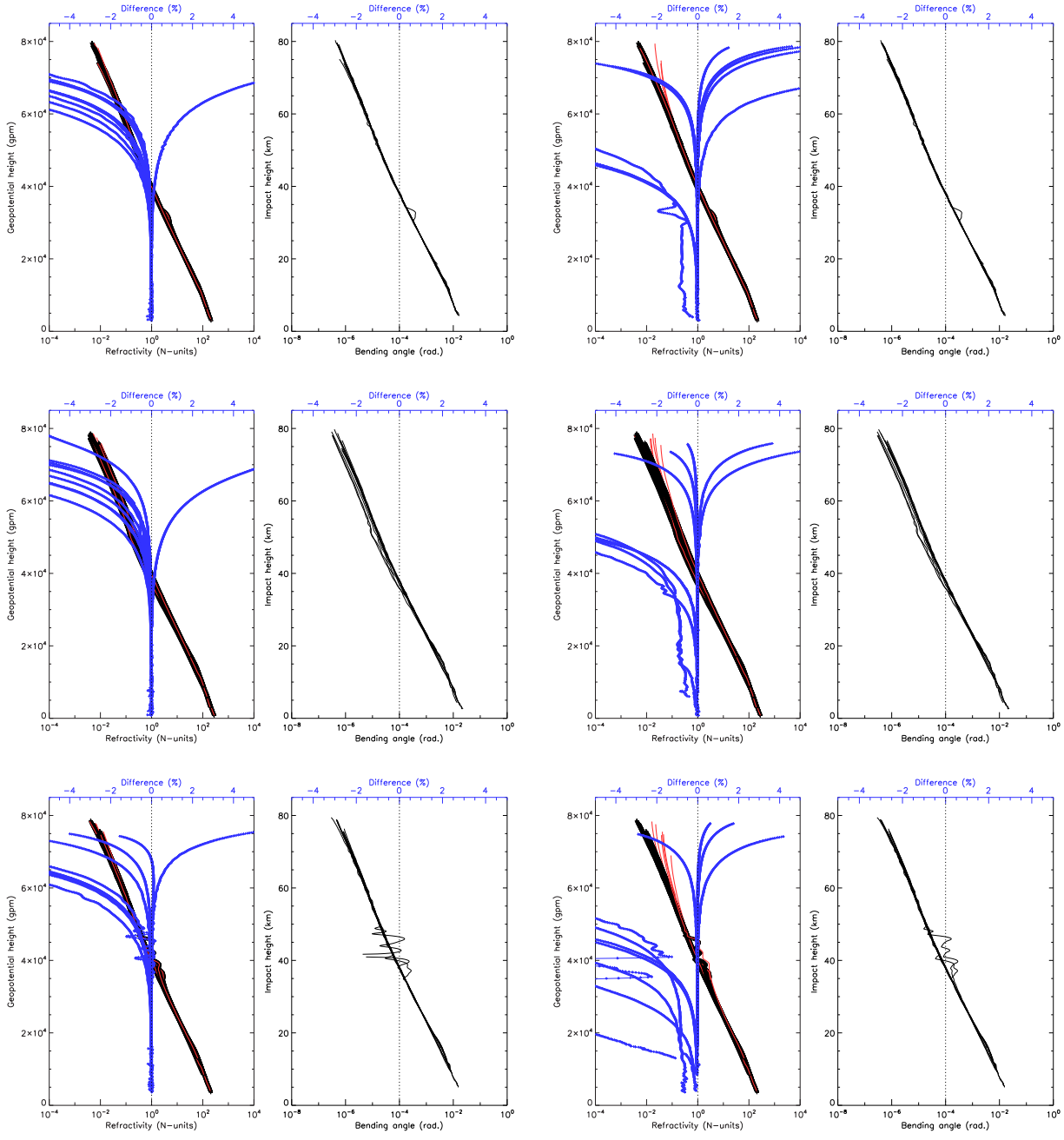


**Figure 2.4:** Sample differences between observed refractivity profiles and the results of successive Abel transform to bending angle and Abel inversion back to refractivity. (a) 'linear' algorithms, (b)'exponential' algorithms.

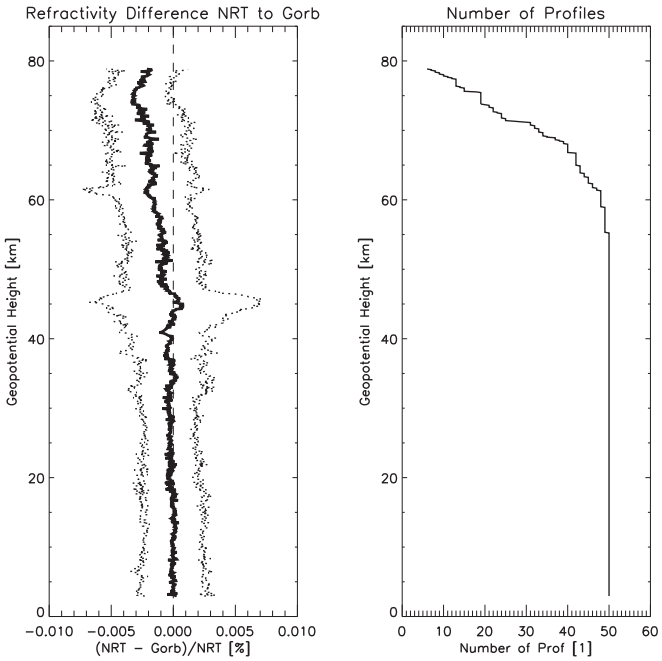


**Figure 2.5:** Difference between ionospheric corrected bending angle and refractivity profiles computed using ROPP (’linear’ algorithm) and the NRT processing product from the GRAS SAF. The bias between results from 50 sample profiles is plotted as a solid line, dotted lines indicate 1 standard deviation. Note the change of scale between (a) and (b).

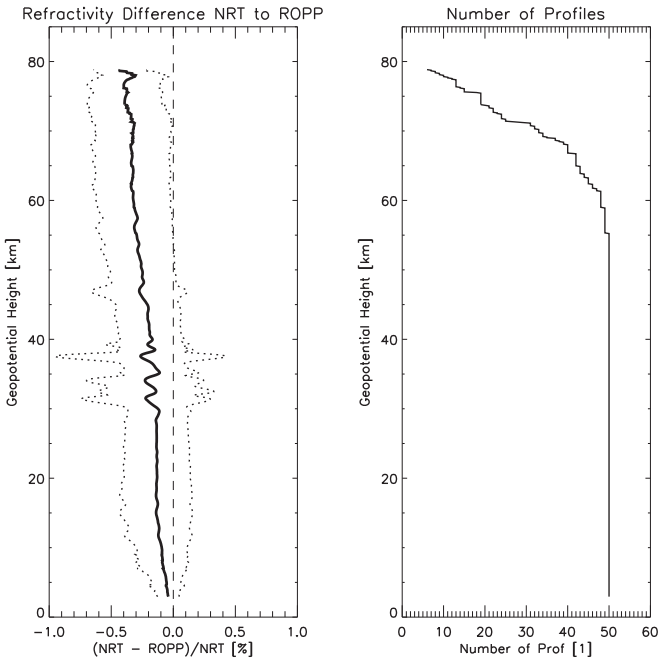


**Figure 2.6:** Difference between ionospheric corrected bending angle and refractivity profiles computed using ROPP (’exponential’ algorithm) and the NRT processing product from the GRAS SAF. The bias between results from 50 sample profiles is plotted as a solid line, dotted lines indicate 1 standard deviation. Note the change of scale from Figure 2.5.

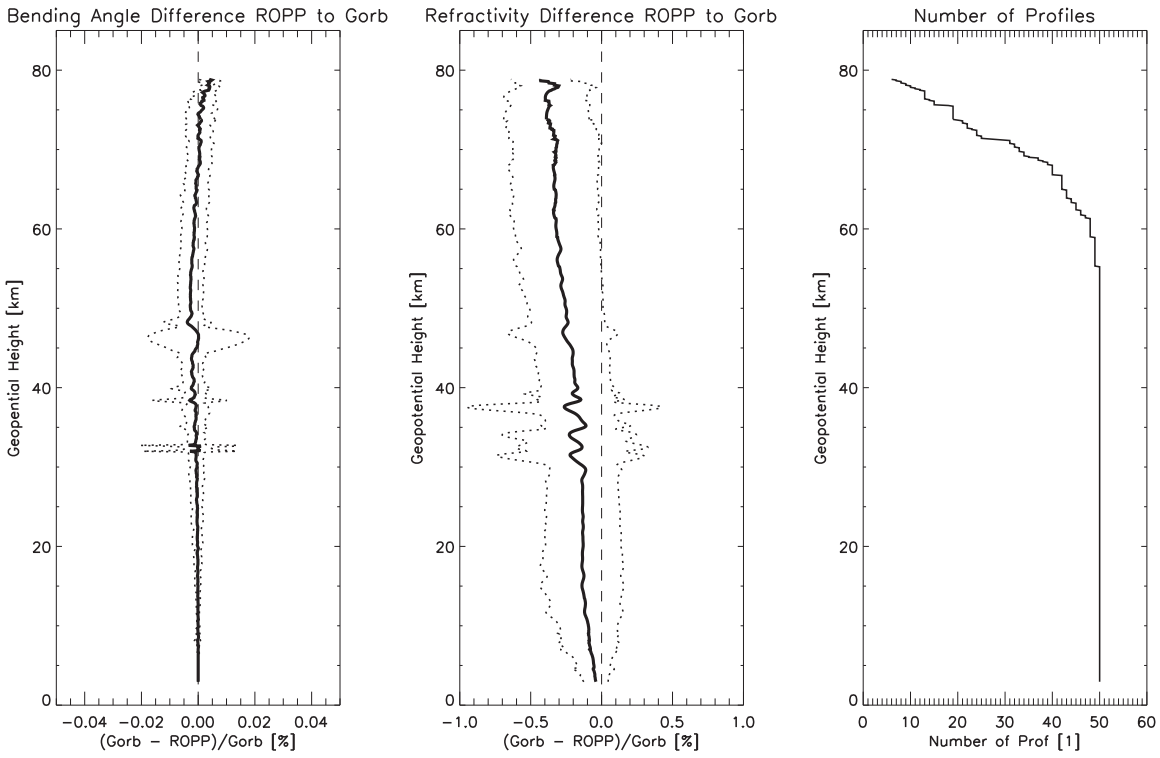


**Figure 2.7:** Difference between ionospheric corrected bending angle and refractivity profiles computed using 'linear' and 'exponential' (ROPP) Abel integral algorithms. The bias between results from 50 sample profiles is plotted as a solid line, dotted lines indicate 1 standard deviation.

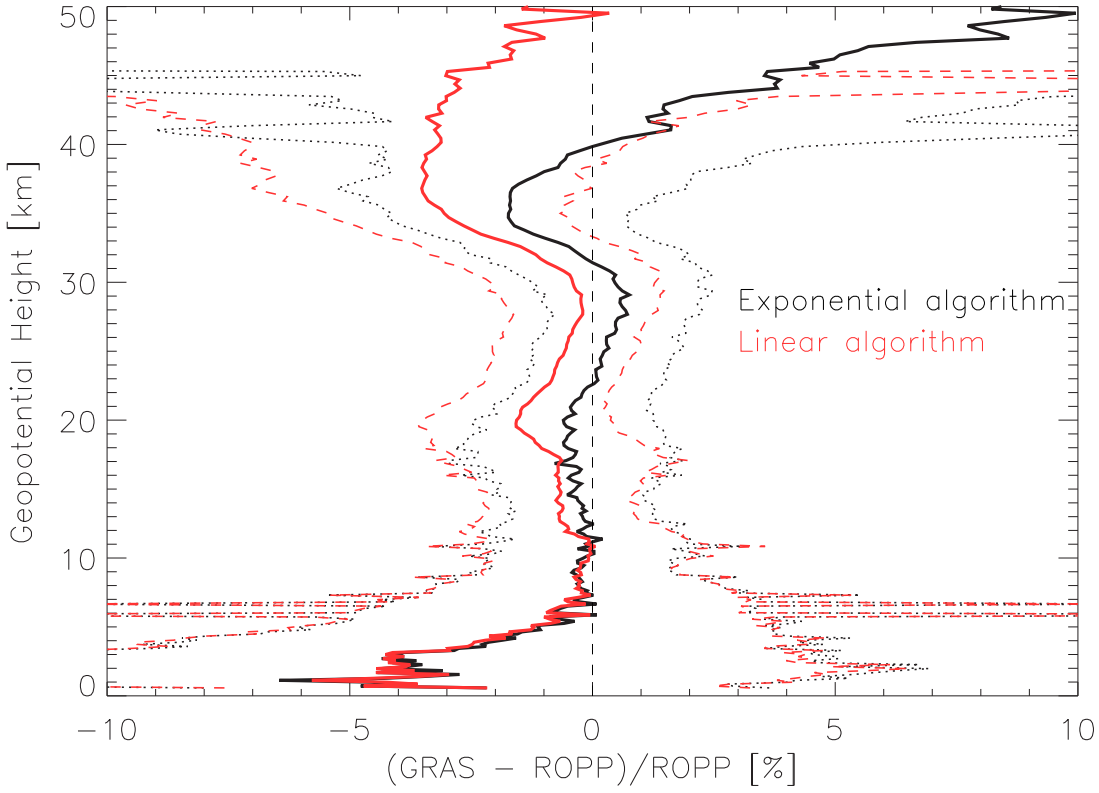


**Figure 2.8:** Differences between observed bending angle and forward modelled background (O-B). The bias between results from 1000 randomly selected GRAS sample profiles and co-located Met Office model data is plotted as a solid line, dotted lines indicate 1 standard deviation. Results in black use the 'exponential' forward Abel transform, results in red use the 'linear' algorithm.

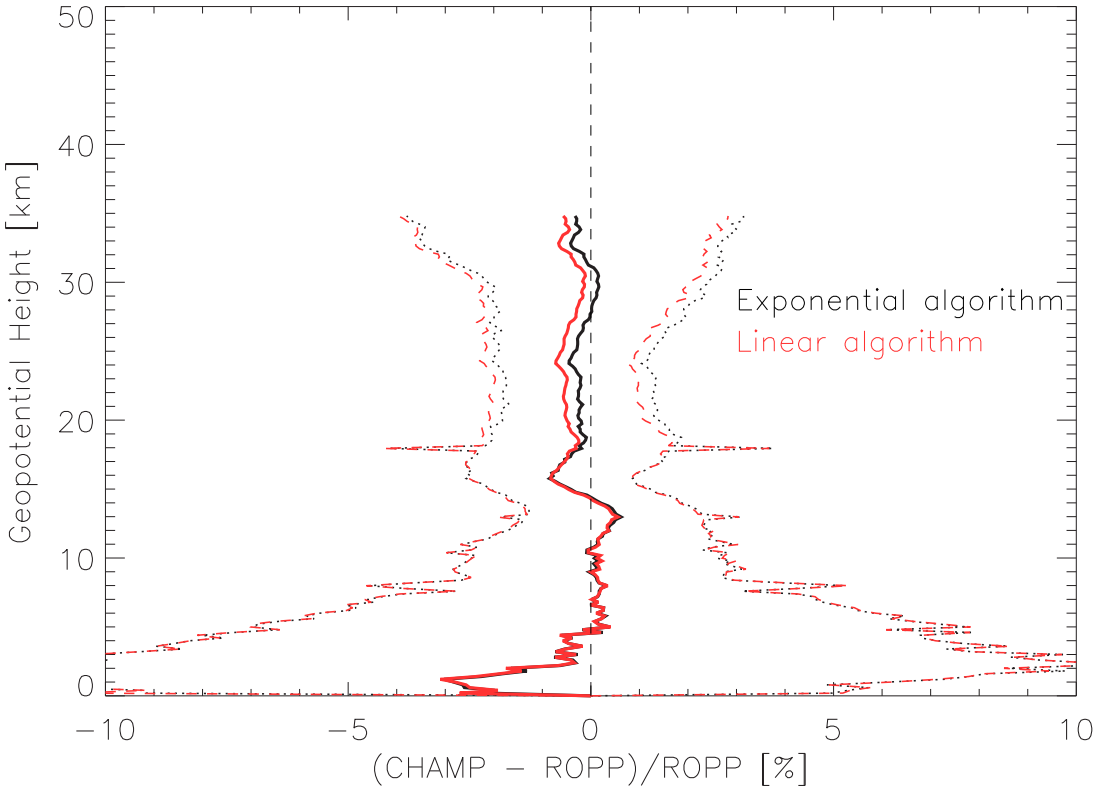


**Figure 2.9:** Differences between observed bending angle and forward modelled background (O-B). The bias between results from 1000 randomly selected CHAMP sample profiles and co-located ECMWF model data is plotted as a solid line, dotted lines indicate 1 standard deviation. Results in black use the 'exponential' forward Abel transform, results in red use the 'linear' algorithm.

# 3 Summary

These tests indicate that the performance of the `ropp_pp` module for processing measured L1 and L2 bending angles to corrected bending angle and refractivity profiles is equivalent to that currently conducted by the GRAS SAF using pre-existing software. This is because `ropp_pp` includes an implementation of the 'linear' Abel integral algorithms developed for the GRAS SAF NRT processing (Gorbunov, 2002).

The `ropp_pp` module also includes some forward Abel transform and inverse Abel routines based on the Abel integral solutions developed by the GRAS SAF for use in the ROPP forward model (`ropp_fm`). This 'exponential' approach assumes exponential variation of bending angle or $\ln n$ between successive observation levels. Use of the 'exponential' algorithms leads to a difference of up to 0.5% in the corrected refractivity profiles compared with current NRT products generated by the GRAS SAF. In the interests of consistency with the GRAS SAF processing, it is recommended that users apply the 'linear' Abel integral algorithms included in `ropp_pp` for pre-processing. A configuration option is provided in `ropp_pp` so that users may choose to apply either method to data processing. For further details refer to the ROPP User Guide (GRAS SAF, 2009).

To achieve the best agreement between observations and forward modelled results, it is recommended that users apply the 'exponential' Abel integrals included in `ropp_fm` for the forward modelling of background data.

The results shown in Figures 2.4 and 2.3 demonstrate the limitations of the assumptions used in both sets of algorithms, and of the sensitivity of calculations to the infinite upper boundary in the Abel integral. The combination of observed data with model bending angles above the top of the observed profile in the `ropp_pp` processing routines limits the influence of this sensitivity on the resulting corrected bending angle and refractivity profiles in the region of interest.

Further development work may be possible to refine the Abel integral algorithms included in future versions of ROPP. In particular, development of the 'linear' algorithm to compute bending angle profiles on different output impact parameters is required for a more representative comparison of its performance in the forward model.

# Bibliography

Abramowitz, M. and Stegun, I., eds., *Handbook of mathematical functions*, Dover, 1965.

Fjeldbo, G., Kliore, G., and Eshleman, V., The neutral atmosphere of Venus as studied with the Mariner V radio occultation experiments, *Astron. J.*, *76*, 123–140, 1971.

Gorbunov, M., Radio-holographic analysis and validation of Microlab-1 radio occultation data in the lower troposphere, *J. Geophys. Res.*, *107*, 10.1029/2001JD000 889, 2002.

Hedin, A., Extension of the MSIS thermosphere model into the middle and lower atmosphere, *J. Geophys. Res.*, *96*, 1159–1172, 1991.

Kursinski, E., Hajj, G., Schofield, J., Linfield, R., and Hardy, K., Observing earth's atmosphere with radio occultation measurements using the Global Positioning System, *J. Geophys. Res.*, *102*, 23.429–23.465, 1997.

Melbourne, W., Davis, E., Duncan, C., Hajj, G., Hardy, K., Kursinski, E., Meehan, T., and Young, L., The application of spaceborne GPS to atmospheric limb sounding and global change monitoring, Publication 94–18, Jet Propulsion Laboratory, Pasadena, Calif., 1994.

GRAS SAF, The Radio Occultation Processing Package (ROPP) User Guide. Part III: Preprocessor module, SAF/GRAS/METO/UG/ROPP/004, Version 4.0, 2009.

### GRAS SAF Reports

| | |
|---|---|
| SAF/GRAS/METO/REP/GSR/001 | Mono-dimensional thinning for GPS Radio Occulation |
| SAF/GRAS/METO/REP/GSR/002 | Geodesy calculations in ROPP |
| SAF/GRAS/METO/REP/GSR/003 | ROPP minimiser - minROPP |
| SAF/GRAS/METO/REP/GSR/004 | Error function calculation in ROPP |
| SAF/GRAS/METO/REP/GSR/005 | Refractivity calculations in ROPP |
| SAF/GRAS/METO/REP/GSR/006 | Levenberg-Marquardt minimisation in ROPP |
| SAF/GRAS/METO/REP/GSR/007 | Abel integral calculations in ROPP |
| SAF/GRAS/METO/REP/GSR/008 | ROPP thinner algorithm |
| SAF/GRAS/METO/REP/GSR/009 | Refractivity coefficients used in the assimilation of GPS radio occultation measurements |
| SAF/GRAS/METO/REP/GSR/010 | Latitudinal Binning and Area-Weighted Averaging of Irregularly Distributed Radio Occultation Data |
| SAF/GRAS/METO/REP/GSR/011 | ROPP 1dVar validation |

GRAS SAF Reports are accessible via the GRAS SAF website http://www.grassaf.org.